Modeling Axial Mixing of Fuel Particles in the Dense Region of a Fluidized Bed

energy&fuels

pubs.acs.org/EF Article

Modeling Axial Mixing of Fuel Particles in the Dense Region of a Fluidized Bed

Anna Köhler,* David Pallarès, and Filip Johnsson

Cite This: *Energy Fuels* 2020, 34, 3294−3304

Read Online

ACCESS | Metrics & More | Article Recommendations

ABSTRACT: A semiempirical model for the axial mixing of fuel particles in the dense region of a fluidized bed is presented and validated against experimental magnetic particle tracking in a fluid-dynamically downscaled fluidized bed (Köhler et al. *Powder Technol.*, 2017, *316*, 492−499) that resembles hot, large-scale conditions. The model divides the bottom region into three mixing zones: a rising bubble wake solid zone, a zone with sinking emulsion solids, and the splash zone above the dense bed. In the emulsion zone, which is crucial for the mixing, the axial motion of the fuel particle is shown to be satisfactorily described by a force balance that applies experimental values from the literature and an apparent emulsion viscosity of Newtonian character. In contrast, the values derived from the literature for key model parameters related to the bubble wake zone (such as the upward velocity of the tracer), which are derived from measurements carried out under cold laboratory-scale conditions, are known to underestimate systematically the measurements relevant to hot large-scale conditions. When applying values measured in a fluid-dynamically downscaled fluidized bed (Köhler et al. *Powder Technol.*, 2017, *316*, 492−499), the modeled axial mixing of fuel tracers shows good agreement with the experimental data.

1. INTRODUCTION

Fluidized bed (FB) units have been used commercially for the combustion and gasification of solid fuels since the early 1970s.[2] Solid fuel conversion uses the two existing types of FB units: bubbling fluidized beds (BFBs) and circulating fluidized beds (CFBs). CFB units differ from the more basic BFB units in that they are operated at higher fluidization velocities, yielding higher levels of specific fuel conversion for a given cross-sectional area, making them suitable for application at larger scales (up to several hundreds of megawatts).[2] The higher investment costs associated with CFB units (e.g., a cyclone and solid recirculation system are needed to prevent the entrained solids to escape the system) are compensated with higher combustion efficiency. BFB boilers are preferably used for lower thermal capacity and thus typically fed with local fuels with higher transport costs in terms of energy density (such as waste and biomass). Despite their obvious design and operational differences, BFB and CFB units for solid fuel conversion use Geldart B group solids[3] as the bed material, yielding the formation of bubbles at the bottom grid of the reactor, which travel upward through a dense bed. In this situation, the dense region in the lower part of the unit, which is the focus of the present work, has been shown to behave similarly in both types of units in terms of fluid dynamics (see, for example, the work of Svensson et al.[4]), albeit with the appearance of a more intense "exploding type" bubble flow in the CFBs than in the BFBs. Thus, as BFB and CFB units for large-scale solid fuel conversion involve similar underlying mechanisms for the mixing of the solids (both bed materials and fuel particles) in the bottom region, the present work is of relevance for both types of units.

The axial mixing of the fuel particles has a strong impact on the fuel conversion rate since the fuel that is immersed in the dense bed and the fuel that is located at the dense bed surface experience different heat and mass transfer phenomena. For the fuel located at the dense bed surface, the presence of fewer bulk particles in the surrounding milieu leads to enhancement of mass transfer and a decrease in heat transfer, as compared to an immersed fuel particle.[5] It has also been found that char particles that originate from the same fuel have a higher reactivity when devolatilization has occurred inside the dense bed rather than at the surface.[6] Thus, axial fuel mixing affects the fuel conversion rate in several ways. Furthermore, fuel particles at the dense bed surface have been shown to experience faster lateral mixing than immersed fuel,[7] which together with the abovementioned fuel conversion rate emphasizes an important aspect for consideration during furnace design.

Studies in the literature on the axial mixing of larger particles in a fluidized bed have mainly been experimental in nature. Among the first researchers to study the axial mixing of fuel particles were Nienow et al.,[8] who observed the flotsam behavior, that is, a tendency to settle floating on the dense bed surface, of coal-like particles at low fluidization velocities. Two-dimensional laboratory beds with particle tracking applying

Received: December 4, 2019
Revised: February 11, 2020
Published: February 13, 2020

optical methods have been frequently used in studies that have provided tracer trajectories (and all the flow pattern data derived therefrom).[9−12] Three-dimensional beds require more advanced methods, such as radioactive particle tracking[13,14] or the more recently developed methods like positron emission particle tracking[15] and magnetic resonance imaging.[16] However, the value of such data sampled under cold conditions is limited to a qualitative frame, regarding their applicability to hot conditions.

The combination of modeling and experimental work represents a valuable tool for increasing our understanding of fuel mixing under various FB conditions, with the aim of building design tools for the development and reliable scale-up of FB units.[17] Two main modeling approaches are used to describe large-scale FB units: semiempirical modeling, in which the velocity fields of the gas and bulk solids are not solved by momentum balances but rather by simpler models and assumptions; and computational fluid dynamics (CFD), in which transport equations for mass, momentum, and heat are solved. While semiempirical models are nongeneric in their formulation, they are reliable mainly within the limited (interpolative) ranges given by the empirical content used. Semiempirical models have the advantage that they can simulate the entire process at affordable computational costs (hours), which makes them a powerful tool for design and engineering purposes,[18−20] although there obviously is a reliance on their underlying assumptions and empirical data.[18−20] In contrast, CFD models build on generic equations that are not limited to any given range of operational conditions and provide results for momentum transfer. As a drawback, CFD models for FB units are not yet fully mature, mainly due to difficulties associated with resolving the solid flow structures at the subgrid level. Therefore, they present with some level of uncertainty in the simulation results and are also computationally costly (requiring months of computing if solving conditions relevant for commercial FB boilers).

The present work aims at expanding current knowledge of solid mixing by describing the axial mixing of a large spherical particle (representative of an FB fuel) in the bottom region of a fluidized bed. For this, semiempirical modeling and experimental work are combined. Correlations with data from the literature for the bubble and solid flows are evaluated and used. To describe the motion of a tracer particle that is representative of a typical fuel particle in the emulsion phase, the equation of motion of the particle is solved. The model uses experimental tracer particle data, both original results and data previously obtained by the authors,[1,21] sampled in a 3D fluid-dynamically downscaled unit by means of magnetic particle tracking (MPT). By up-scaling the experimental data, the model can be validated against data relevant to hot industrial-scale conditions, a method, whose results are in good qualitative and quantitative agreement with experiments in actual hot industrial-scale units as shown by Sette et al.[22]

Once validated, the model is used to study the relevancies of different mechanisms and parameters in relation to axial solid mixing.

2. MODELING

The model used to describe axial mixing of the fuel particles in the dense region of a fluidized bed considers not only the splash zone above the dense bed surface but also two distinct zones in the dense bed: (1) the bubble wake zone, which consists of gas in the form of bubbles and bed solids that are dragged upward in the bubble wake; and (2) the bubble-free emulsion zone, in which gas flows upward while bed solids sink so as to compensate for rising wake solids. A schematic of the model showing the movements of the fuel particles, gases, and bulk solids is presented in Figure 1.

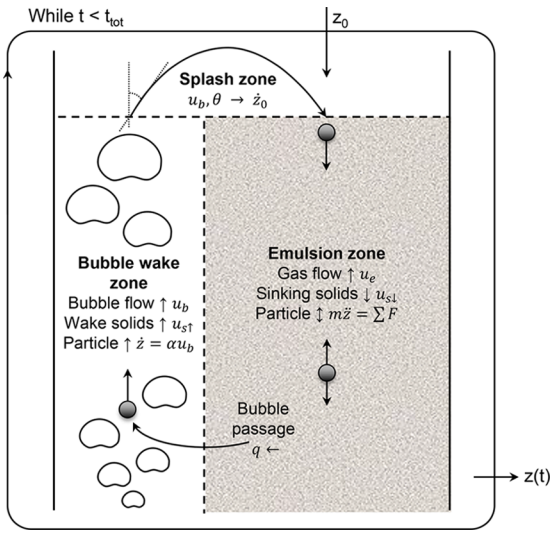

Figure 1. Schematic of the model that describes the mixing of a spherical tracer particle that is representative of a typical fuel particle.

The bubble wake zone is associated with the upward flow of bubbles and solids (including fuel particles), whereas the emulsion zone contains bulk solids that are flowing downward and fuel particles that tend to flow upward or downward, depending on the net balance of forces acting upon them. The splash zone has its origin in the ejection of solids from bubbles erupting at the dense bed surface. The lateral scattering of solids and fuel particles after the ejection will depend on the bubble velocity and a scattering angle.

It is generally accepted in the literature that gas bubbles are the main driving force of solid mixing,[23] while three main mechanisms are identified:[24] wake lifting, solids sinking around the bubbles, and solids scattering through bubble eruption on the bed surface. In this model, all mixing of the bed material and, therefore, fuel particles is assumed to be caused by the ascension of bubbles through the bed and their eruption at the dense bed surface. Thus, an appropriate description of the bubble flow characteristics is crucial for determining the solid mixing.

2.1. Modeling Bubble Flow. Models to describe bubbles in fluidized beds were earlier discussed by Davidson and Harrison,[25] who divided the bed into two phases: a gas flow at the minimum fluidization velocity passing through a particulate phase and becoming a gas−solid emulsion with constant voidage and the remaining gas rising as bubbles through a solid-free gas phase.[26] However, under conditions that are typical for commercial solid fuel conversion units, this approach was found to overestimate the expansion of the bed as a consequence of the bubbles, and the presence of a significant gas throughflow must be considered.[27−29] The presence of the throughflow results in a bubble flow rate lower than in the original theory (where all the excess gas contributes to the bubble flow), while the gas−solid emulsion is still at the minimum fluidization velocity. Thus, the total gas flow into the bed is the sum of the flow through the emulsion phase, the

https://dx.doi.org/10.1021/acs.energyfuels.9b04194
Energy Fuels 2020, 34, 3294−3304

visible bubble flow, and the throughflow, and it can be expressed as

$$u_o = u_{mf} + u_{vis} + u_{tf} \quad (1)$$

The visible bubble flow can be expressed with the volume fraction of the bubble phase, commonly denoted as bubble density δ

$$u_{vis} = \delta u_b \quad (2)$$

In the original two-phase theory, the bubble rise velocity in beds with multiple bubbles was given by superimposing the rise velocity of a single bubble in a large bed with the excess gas velocity used to fluidize the bed. Considering the throughflow,[29] the bubble rise velocity results in

$$u_b = u_o - u_{mf} - u_{tr} + u_{br} \quad (3)$$

Based on an early theoretical derivation of the rising velocity of a single bubble released in a liquid,[30] Davidson and Harrison[25] compared different empirical expressions for a single bubble in a large bed at the minimum fluidization, and they suggested an expression that subsequently has entered common usage

$$u_{br} = 0.711 \times \sqrt{g \times D_b} \quad (4)$$

where D_b is the equivalent diameter of a sphere with the same volume as the bubble cap.

There are many different expressions for the bubble diameter in the literature.[23,31−33] The bubble diameter increases up through the bed, mainly as a result of coalescence with other bubbles. In this work, the correlation of Darton et al.[32] is used to predict the bubble diameter, which is particularly suitable for freely bubbling beds, considering growth by coalescence with other bubbles, and it is found to correlate well with the experimental data from other authors.[29] The equation for the bubble diameter is

$$D_b = 0.54 g^{-0.2} (u_o - u_{mf})^{0.4} \times (z + 4\sqrt{A_0})^{0.8} \quad (5)$$

Incorporating the bubble diameter of Darton et al.[32] into eq 4 gives

$$u_{br} = 0.52 g^{0.4} (u_o - u_{mf})^{0.2} \times (z + 4\sqrt{A_0})^{0.4} \quad (6)$$

where z is the vertical location of the bubble, and A_0 is the bubble catchment area (a grid design parameter).

As for the bubble density, combining eqs 1−3 yields

$$\delta = \frac{1}{1 + \frac{u_{br}}{u_o - u_{mf} - u_{tf}}} \quad (7)$$

where u_{tf} is the throughflow, which is found to be relevant from excess velocities above 0.19 m/s. The bed voidage along the dense bed height and, therefore, the bubble density, is constant, as shown by time-averaged pressure measurements inside the dense bed, yielding a linear pressure drop over the bed height.[4] With this, the basis for an expression that describes the throughflow is obtained from eq 7[29]

$$u_{tf} = (1 - f_2 (z + 4\sqrt{A_0})^{0.4})(u_o - u_{mf}) \quad (8)$$

where f_2 is an empirical expression derived from experiments. Johnsson et al.[29] used bed voidage measurements in a large-scale bubbling fluidized bed under hot conditions to correlate the following expression for f_2

$$f_2 = [0.26 + 0.70 \exp(-0.0033 D_s)] \times [0.15 + (u_o - u_{mf})]^{-0.33} \quad (9)$$

where D_s is the average diameter of the bed solids. Their experiments covered sand of various particle diameters (0.15−0.79 mm) and fluidization velocities from 0.02 m/s and up to 3 m/s.

Finally, the bubble velocity, u_b, can be extracted from the description of the bubble flow and used to simulate the mixing of a fuel particle.

2.2. Modeling Fuel Mixing. Below, the modeling expressions describing the axial mixing of a fuel particle (i.e., a spherical particle that is larger and lighter than the bed particles) in the different zones considered in Figure 1 are given. The order followed is that of a mixing cycle: starting with the rise of the fuel particle caused by wake solids, it is eventually ejected into the splash zone, lands back on the dense bed surface, and immerses the dense bed to, at some point, be caught up by a new bubble wake, thus closing the cycle.

The model is implemented as dynamic Lagrangian tracking with time marching:[34] in each timestep (which is in the order of 10^{-2} s), the acceleration of the single fuel particle is determined from which the velocity, the axial location, and the phase containing the fuel particle in the next timestep can be derived. Like this, the trajectory of the particle is obtained, while the dynamic simulation is run until sufficiently robust statistics are achieved (typically after simulated times in the order of 10^3 s). The acceleration or velocity of the fuel particle respectively is determined differently dependent on the zone the particle is located in.

2.2.1. Bubble Wake Zone. Within the bubble wake zone, the rise velocity of the fuel particle is slower than that of the bubbles as it is typically not dragged up in a single bubble wake but undergoes consecutive joining and detaching from different wake regions. Thus, the velocity of the fuel particle is expressed as a fraction of the bubble rise velocity, as expressed in eq 10

$$u_p = \alpha \times u_b \quad (10)$$

The values of α are discussed in connection to the experimental work described in Section 3.

2.2.2. Splash Zone. Once the fuel particle in the bubble wake reaches the dense bed surface, it is ejected into the splash zone by the erupting bubble. The vertical component of the ejection velocity of the tracer depends on the bubble velocity at the dense bed height and the ejection angle, θ, which is in the range of 0−90°

$$u_{start} = u_b|_{z=H_b} \times \cos(\theta) \quad (11)$$

The model considers a scatter in eq 11 based on experiments,[35] showing that the ratio of the experimental mean values of the left- and right-hand sides of eq 11 follows a Gaussian distribution, with a mean of 1 and a standard deviation of 0.32. The probability density function of the ejection angle, θ, is also taken from these experiments[35]

$$p(\theta) = 0.046 \exp(-0.045\theta) \quad (12)$$

Having a certain vertical component of the ejection velocity, the particle is assumed to follow a ballistic movement in the splash zone, with gravity as the sole force. Thus, the ejected

https://dx.doi.org/10.1021/acs.energyfuels.9b04194
Energy Fuels 2020, 34, 3294−3304

particle eventually lands back on the dense bed surface, where it joins the emulsion zone with the sinking solids.

2.2.3. Emulsion Zone and Sinking Solids. The motion of a fuel particle in the emulsion zone, in terms of acceleration, is defined by the sum of the forces acting on it, that is, the gravitational, buoyancy, and drag forces, which can be expressed as

$$a_p = \left(\frac{\rho_e}{\rho_p} - 1\right) \times g + \frac{3\rho_e C_D}{4\rho_p D_p} |(u_{s\downarrow} - u_p)| \times (u_{s\downarrow} - u_p) \quad (13)$$

While the gravitational and buoyancy forces (represented by the first right-hand term in eq 13) consist of known variables, determination of the drag force (second right-hand term) requires knowledge of the velocity of the sinking bulk solids. From a mass balance performed on the bulk solids, the resulting velocity of the sinking solids is given by

$$u_{s\downarrow} = \frac{f_w \times \delta \times u_b}{(1 - \delta - f_w \delta)} \quad (14)$$

where f_w is the wake volume fraction of the rising bubbles.[23] The values for this parameter are available from experiments using Geldart B particles of various sizes and densities.[36]

Regarding the drag force, the drag coefficient acting on the fuel particle can be calculated from the Reynolds number knowing the regime of the flow around the particle. For $Re > 0.5$, the flow might separate from the fuel particle, so for this transition regime, a common correlation used for spherical particles is that proposed by Schiller and Naumann[37]

$$C_D = \frac{24}{Re}(1 + 0.15Re^{0.687}) \quad (15)$$

The Reynolds number is calculated by assuming that the emulsion zone has a Newtonian character such that a constant apparent viscosity is used. This assumption is based on experimental findings with the falling sphere method conducted in a cold laboratory-scale bed of sand by Rees et al.,[38] which were further supported by experiments performed by the authors.[21] The present work uses an up-scaled value for the viscosity of the gas−solid emulsion of 1.24 Pa s, as determined by Rees et al.[38]

The force balance in eq 13 may be extended by an additional lift force that results from the formation of endogenous bubbles[39] as high fluxes of gas (moisture and volatiles) are released from the fuel particle during the first conversion stages. The lift force related to this effect is expressed as[39]

$$F_{lift} = 0.372 g^{3/5} \rho_e D_p Q^{4/5} \quad (16)$$

where Q is the volume flow of the gases released from the particle, in which if one assumes a constant release, the rate can be calculated using the proximate fuel composition and a characteristic time for simultaneous drying and devolatilization. Here, for simplicity, an experimental correlation is used to estimate this characteristic time[40]

$$\tau_{vol} = 12.08 \times 10^4 D_p^{1.44} T^{-1.61} \quad (17)$$

With the given force balance (eq 13) and expressions for the drag force, a theoretical investigation is made of the height in the bed at which the forces acting on the still fuel particle (i.e., the particle velocity is zero) balance out. In other words, this is the height at which the studied particle would end up if it was not captured by rising bubble wakes. This provides a clearer picture of the impacts that different parameters have on the force balance. Figure 2 shows the influences of tracer particle size (big tracer), density (biochar tracer), and bed viscosity (high viscosity) on this balancing height with increasing fluidization velocity. As a reference case, published[38] values for the viscosity and wake fraction (μ_0 = 0.5 Pa s; f_w = 0.38) were taken, and a biomass spherical particle (4 cm, 813 kg/m^3) was used. Increasing the viscosity to 5 × μ_0 yields an increase in drag force, shifting a certain balancing height to lower fluidization velocities. A lighter (biochar) or larger tracer requires a higher fluidization velocity to reach a given balancing height as the buoyancy force becomes more pronounced.

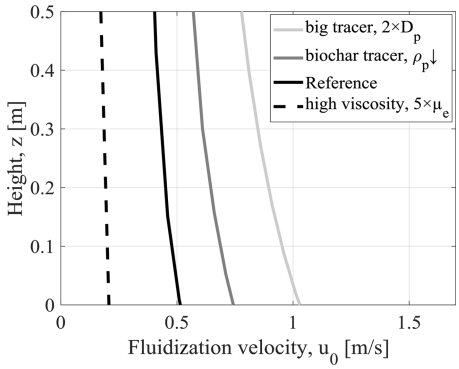

Figure 2. Balancing height in the bed (calculated using eq 13) versus fluidization velocity for various tracer sizes and densities and apparent bed viscosities. Reference case: fresh biomass, 4 cm in diameter, 810 kg/m^3, and μ_e = 1.23 Pa s.

Furthermore, the expressions listed in this subsection can be used to estimate what is here termed the "immersion velocity", that is, the threshold value of the fluidization velocity for which the fuel particle will start to experience sufficient drag from the bulk solids to become immersed in the bed and therefore transition from a purely flotsam behavior. Figure 3 shows the dependencies of the immersion velocity on bed height, shown to have little influence, and on the particle diameter and density, which yield a higher immersion velocity when increased and decreased, respectively. Note that while higher

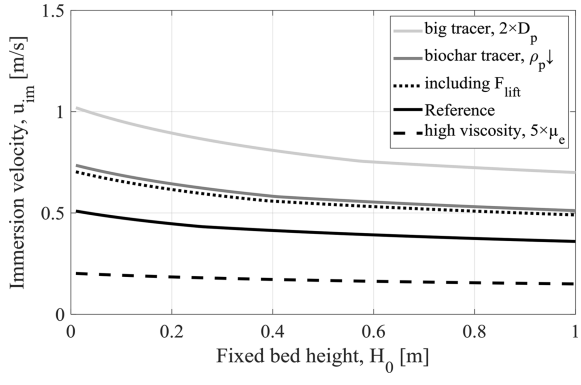

Figure 3. Immersion velocity (calculated from eq 13 versus fixed bed height, tracer size and density, apparent bed viscosity, and added lift force (F_{lift}). Reference case: fresh biomass, 4 cm in diameter, 810 kg/m^3, and μ_e = 1.23 Pa s.

https://dx.doi.org/10.1021/acs.energyfuels.9b04194
Energy Fuels 2020, 34, 3294−3304

dense beds yield larger splash zones, the splash zone itself does not have any net contribution in terms of solid flow, that is, the same flow of solids entering it by splashing is leaving it back to the bed surface by gravity.

2.2.4. Transfer between the Emulsion and Bubble Wake Zones. The probability that the fuel particle will transfer from the bubble wake zone to the sinking solid emulsion zone was evaluated from experimental data acquired in a previous study.[1] Characterized by very low measured probability values, the mechanism was identified as playing a negligible role in the axial mixing of the studied tracers (resembling fuel particles) and was therefore not considered in the modeling. Instead, the transfer from the bubble wake to the emulsion zone was considered to occur exclusively through an indirect path involving ejection of the fuel particle into the splash zone and subsequent landing on the dense bed surface, that is, the emulsion zone.

From the same experimental data,[1] but investigating the opposite direction, when located in the emulsion zone, the fuel particle was likely to be captured by the wake region of passing bubbles and to start to rise, thereby being dragged into the bubble wake zone. This transfer from the emulsion zone into the rising bubble wake zone is considered to occur with a probability, q, each time a bubble passes the bed height at which the particle is located.[11] Obviously, high probability values imply short residence times in the sinking solid phase and thus low immersion depth. These q values can be extracted from experimental data, as discussed in Section 3.3.

2.3. Modeling a Converting Biomass Particle. Finally, the axial mixing of a biomass particle undergoing conversion is simulated by introducing two conversion stages: (i) drying and devolatilization and (ii) char combustion. In the first stage, the moisture and volatiles are released from the particle and create a lift force acting on the particle, as described previously. A shrinking density model is assumed, with the particle density ρ_p decreasing linearly from the fresh biomass density ρ_I to the biochar density ρ_{II}, while the particle diameter is assumed to be constant

$$\rho_p(t) = \frac{(\rho_I - \rho_{II})}{\tau_{vol}} t + \rho_I \tag{18}$$

For the second stage, that is, char conversion, a shrinking sphere model is assumed, which yields a constant particle density equal to that achieved after the first conversion stage, that is, the biochar density, and a particle diameter that decreases according to

$$\frac{dD_p}{dt} = -4\Omega \frac{D_{AB}}{D_p \rho_{II}} C_{O2\infty} \tag{19}$$

where Ω is the stoichiometric coefficient, which has a value of 2 when assuming complete conversion. $C_{O2\infty}$ is the oxygen concentration distant from the particle, which is assumed to be 15%, and D_{AB} is the diffusivity of oxygen in nitrogen, which is taken as 2.07×10^{-4} m^2/s. The time of char conversion is calculated by integrating eq 18 from zero to infinity

$$\tau_{char} = \frac{\rho_{II} D_p^2}{8\Omega D_{AB}} C_{O2\infty} \tag{20}$$

Together with the time of drying and devolatilization, the time of char conversion contributes to the total modeling time of the converting biomass particle.

3. EXPERIMENTAL WORK

The experimental data to be used as input and validation data in the semiempirical model are extracted from the measured trajectories of spherical tracer particles in a fluid-dynamically downscaled fluidized bed.[1]

3.1. Experimental Setup. The trajectories, from which tracer distributions and velocity fields can be extracted, were obtained by MPT, a method previously presented by the authors,[41] which uses anisotropic magnetoresistive (AMR) sensors to measure the variation of an electric field generated by the permanent magnet used as the tracer. In the study, four three-axis AMR sensor assemblies are mounted at each side of the squared bed, generating a measurement point by 4 × 3 sensors. The overdetermined system with five variables (position in three dimensions and orientation) is then solved by minimizing the squared difference between the modeled and measured magnetic field. For further details on the measurement technique, the reader is referred to the study of Sette et al.[42]

The fluid-dynamically downscaled bed (0.17 × 0.17 m^2 in cross section), which consisted of fine bronze particles, was fluidized with ambient air. Applying fluid dynamic scaling as described by Glicksman et al.,[43] this resembles a 0.74 × 0.74 m^2 bed with 250 μm sand/ash (2600 kg/m^3) fluidized with air at 800 °C. The gas distributor was a perforated plate with a low pressure drop, maintaining the distributor-to-bed pressure ratio typically seen in large-scale units. The tracer particles were spherical with densities corresponding to those of (i) the bed emulsion at the minimum fluidization velocity (neutrally buoyant), (ii) fresh biomass, and (iii) a light biochar particle. The results extracted from the neutrally buoyant tracer are used to extract values for empirical parameters in the modeling: the probability to start rising, q. After this, tests with tracer particles representing fresh biomass and biochar particles are used to validate the model. Table 1 gives general information about the main parameters of the experimental setup. Note that the data presented in this paper always relate to hot up-scaled conditions.

Table 1. Main Parameters Used in the Experimental Setup

parameter	ambient conditions	hot up-scaled conditions
temperature (°C)	20	800
fixed bed height (m)	0.07	0.30
minimum fluidization velocity (m/s)	0.024	0.05
fluidization velocity (m/s)	0.028−0.253	0.059−0.528
bed material mean particle diameter (μm)	60	250
bed material solid density (kg/m^3)	8900	2600
tracer diameter (m)	0.01; 0.02; 0.03	0.04; 0.08; 0.12
tracer density (kg/m^3)	1465; 2980; 4320	400; 810; 1180

For the smallest tracers (corresponding to 4 cm on an up-scaled basis), the data were taken from a previous work conducted by the authors,[1] while original experimental data with up-scaled sizes of 8 and 12 cm were generated for the present work.

3.2. Fuel-to-Bubble Velocity Ratio. Previous studies have estimated the velocities of large objects in fluidized beds to be in the range of 10−30% of the bubble velocity.[8−10,12,44] This span in the published values is mainly attributed to the wide variety of units (pseudo-2D and pseudo-3D of various sizes but all operated under cold conditions), solids, and operational conditions applied. However, an original analysis of previous measurements by the authors[1] and with quantitative relevance for hot conditions reveals much higher values for α and a decreasing trend with increasing excess gas velocity, as shown in Figure 4. Here, α is calculated with the measured upward velocity of the tracer and the bubble velocity from eq 3 using the correlation of Darton et al.[32] to predict the bubble diameter averaged over the bed height. Furthermore, for the studied conditions, α is shown to be relatively independent of the tracer density.

https://dx.doi.org/10.1021/acs.energyfuels.9b04194
Energy Fuels 2020, 34, 3294−3304

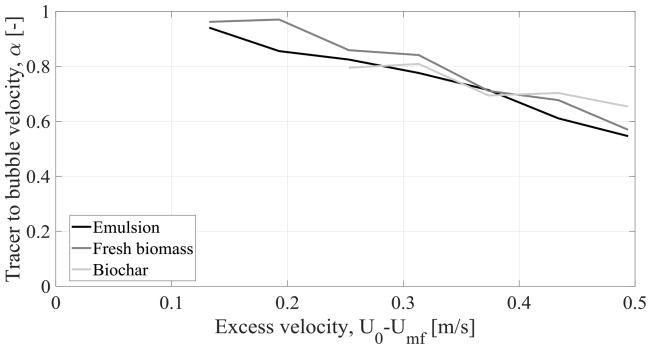

Figure 4. Tracer-to-bubble velocity ratio, α, versus excess gas velocity, $u_0 - u_{mf}$. Calculated with measured data from three tracer particles (4 cm, 400/810/1180 kg/m^3)[1] and according to eq 3.

3.3. Probability of the Tracer to Start Rising. Figure 5 shows the probability q for a spherical tracer of 4 cm in diameter and a density of 1180 kg/m^3 (neutrally buoyant) to start rising in the bed. The fixed bed height was around 30 cm, and the fluidization velocities ranged from 0.12 to 0.54 m/s. It is assumed that under these bubbling conditions, the axial mixing is not strongly affected by the presence of the walls, as there were 2 × 2 bubble paths obtained, and no slagging was observed. To find q the valleys of the time series of the vertical position of the tracer are extracted, that is, this is where the tracer starts to rise. Valleys with a prominence less than 1.5 cm are ignored to make sure that only circulation of the tracer is captured and small vibrations and floating are filtered out. The number of valleys in each horizontal slice is normalized with the total number of found valleys, the measurement frequency, and the bubble frequency at the studied height.

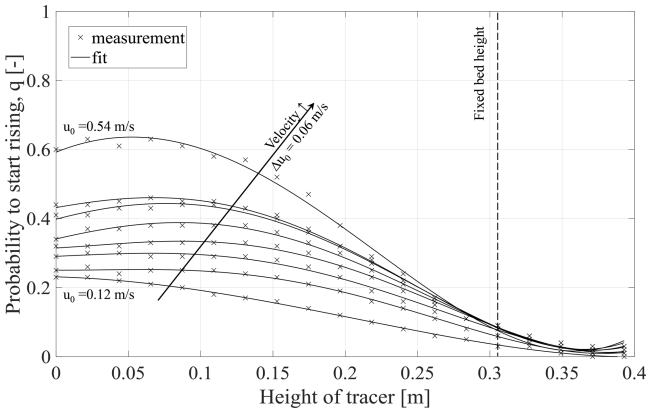

Figure 5. Measured probabilities to transfer from the sinking emulsion to the bubble wake solid zone, q. Tracer particle: D_p = 4 cm, ρ_p = 1180 kg/m^3, H_0 = 30 cm, and u_0 = 0.06−0.54 m/s.

As shown in Figure 5, the probability that the particle will transfer into the bubble wake zone is the highest close to the bottom of the bed and decreases gradually with increasing height in the bed. Increasing the fluidization velocity increases the phase-change probability as the bubbles grow bigger and the bubble density increases, making it more likely that tracer particles will be dragged along. The influences of tracer size and density have also been investigated, although no clear trend for lighter and/or bigger particles was observed. A partial explanation for this is the flotsam behaviors of these tracers, which make it difficult to gather enough representative measurement points inside the dense bed for the cases in which buoyancy forces predominate.

As the goal of this work is to provide a model with easy implementation, the sensitivity of the model results when using different assumptions for the probability to transfer into the bubble wake zone was assessed. The model results for typical conditions were very similar when using the height-resolved probability curves corresponding to each case, constant (height-averaged) probability values corresponding to each case, or the same constant probability value for all the cases. Thus, given this low-level sensitivity, a constant value with a height of q = 0.21 was applied to all the modeled cases.

4. RESULTS

This section summarizes the main findings of the work, starting with model validation against experimental data[1] and then analyzing the sensitivity of the model results for different parameters.

4.1. Model Validation. Figure 6 compares the measured[1] and modeled probability density function (PDF) of the particle axial location for various fluidization velocities and particle densities. Initially, a value for the wake fraction of f_w = 0.94 was obtained by minimizing the squared error between the modeled and measured data. As shown in Figure 6, the model reproduces the trends observed in the experiments, that is, increasing the fluidization velocity results in better axial mixing and lighter particles are more prone to float on the bed surface at low fluidization velocities.

The axial-segregating tendency of the fuel, which, as mentioned in Section 1, is a critical phenomenon in the design of FB units for solid fuel conversion, can be represented as the fraction of time spent by the particle on and above the dense bed surface. In Figure 8, the measured and modeled values for this time share are plotted against the fluidization velocity for two different particle densities. The axial location

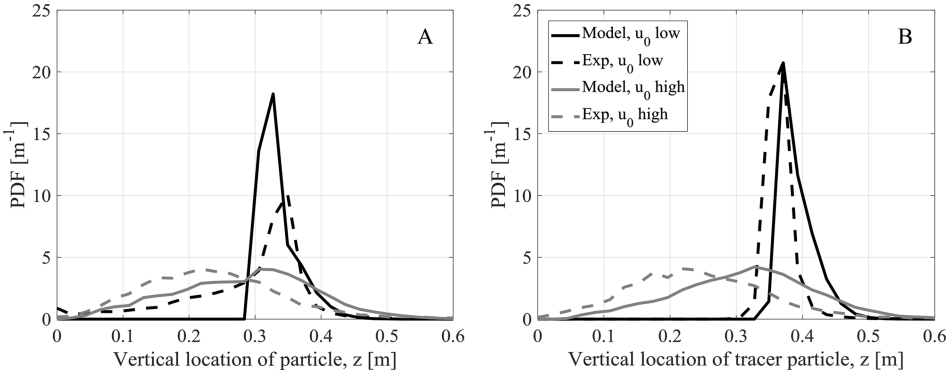

Figure 6. Measured[1] and modeled probability density functions for the vertical location of a fuel particle for two different excess velocities (0.13 and 0.43 m/s). D_p = 4 cm. (A) Fresh biomass. (B) Biochar.

https://dx.doi.org/10.1021/acs.energyfuels.9b04194
Energy Fuels 2020, 34, 3294−3304

of the dense bed surface, that is, the dense bed height, was determined from experiments conducted with a fully flotsam tracer. It should be noted that these experiments did not give a distinct value but a continuous distribution, which reflects the fluctuating nature of the dense bed height due to the strong dynamics. As can be seen in Figure 7, with increasing

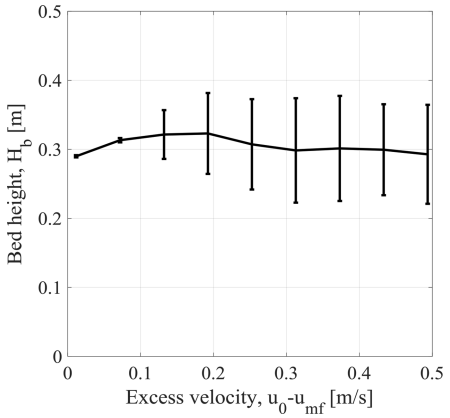

Figure 7. Bed height, H_b (m), versus excess gas velocity, $u_0 - u_{mf}$ (m/s) as obtained from a purely flotsam tracer (1180 kg/m^3, 0.12 m).

fluidization velocity, the bed height is first increased, and fluctuations become higher until the bed height stabilizes around 0.3 m with a standard deviation of around 0.07 m as indicated by the error bars.

In Figure 8, the fraction of time spent by the particle on and above the dense bed surface is corrected with the bed height distribution at each fluidization velocity in the experiments. In the experimental work,[1] three mixing regimes were identified for tracers with typical fuel particle densities (i.e., with a density lower than that of the gas−solid emulsion), which are also reproduced by the modeled data: (1) a purely flotsam regime occurring at low fluidization velocities, (2) a transition regime over which an increase in fluidization velocity results in a rapidly decreased presence of fuel particles at the bed surface, and (3) a fully developed mixing regime in which the presence of particles at the bed surface and the splash zone remains constant with the fluidization velocity. The onset fluidization velocities between the regimes depend mainly on the tracer properties. Note that although the model was able to reproduce the three abovementioned regimes and to provide a PDF for the tracer axial location that was in satisfactory agreement with the experimental results, the fully developed mixing regime of the modeled data has a systematic higher proportion of tracer observations on the bed surface than the corresponding experiments. The main reason for this is that while the model uses a constant dense bed height, this fluctuates strongly in the experiments. In experiments, a tracer particle floating on the dense bed surface when the dense bed is below its time-averaged height will be counted as immersed, which complicates the quantitative comparison between the model and measurements.

4.2. Sensitivity Analysis. To identify the key parameters that influence the axial mixing of fuel particles, the model is used to compare the results from a reference case with those obtained when varying selected parameters. Table 2 gives an overview of the input values used as the reference case in the model. The reference case simulates a fresh biomass particle with 4 cm in diameter and a density of 1230 kg/m^3, while the bed viscosity was set to 1.23 Pa s and the lift force generated from released volatiles was included in the model. Note that as the reference case is different from the validation case and the experiments, the measurement results are not included for comparison.

Table 2. Main Parameter for the Reference Case

temperature	800 °C
bed material density	2600 kg/m^3
bed material size	250 μm
bed height (H_0)	0.3 m
fuel particle diameter (D_p)	0.04 m
fuel particle density (ρ_p)	1230 kg/m^3
timestep	0.02 s
total modeling time	900 s

Figure 9 shows the modeled share of time spent by the biochar fuel particle on and above the dense bed surface as a function of the fluidization velocity for varying apparent viscosities of the emulsion. The viscosity exerts a rather strong influence on the mixing of the fuel particle, with a much higher viscosity, resulting in the fuel starting to be dragged into the bed at lower fluidization velocities and, with an increased

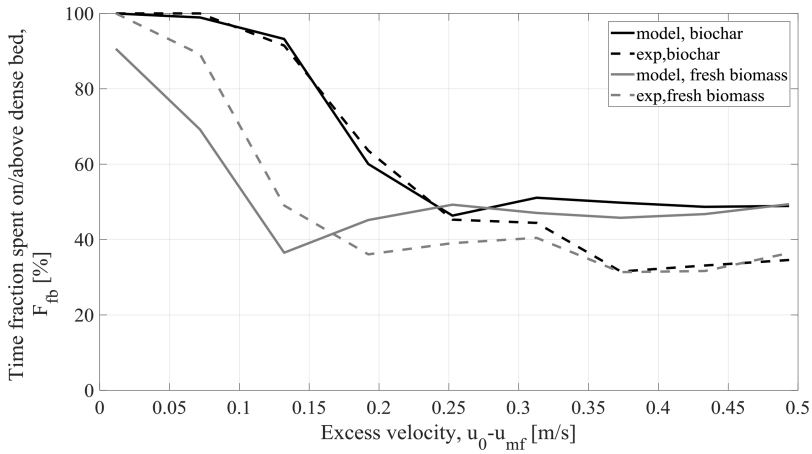

Figure 8. Modeled and experimental time fractions spent by the fuel particle on and above the dense bed surface, F_{fb} (%), versus excess gas velocity, $u_0 - u_{mf}$ (m/s) for varying fuel density (see Table 1).

https://dx.doi.org/10.1021/acs.energyfuels.9b04194
Energy Fuels 2020, 34, 3294−3304

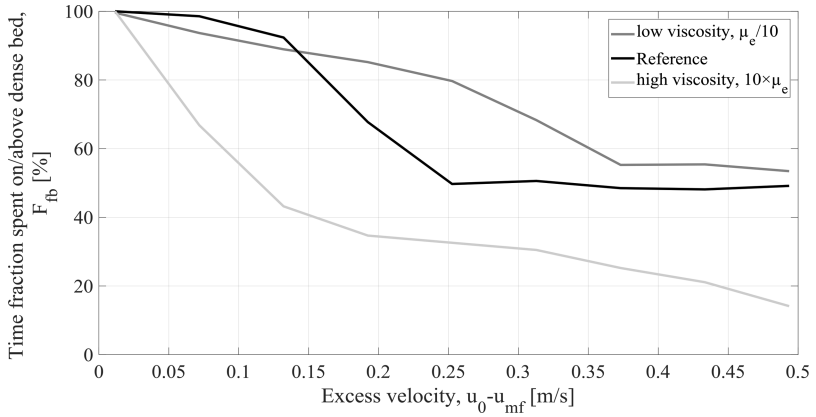

Figure 9. Modeled influence of the apparent viscosity of the emulsion on the time fraction that the fuel particle spends on or above the bed surface, F_{fb} (%), versus the excess velocity, $u_0 - u_{mf}$ (m/s). Reference case: fresh biomass, 4 cm in diameter, and μ_e = 1.23 Pa s, including lift force.

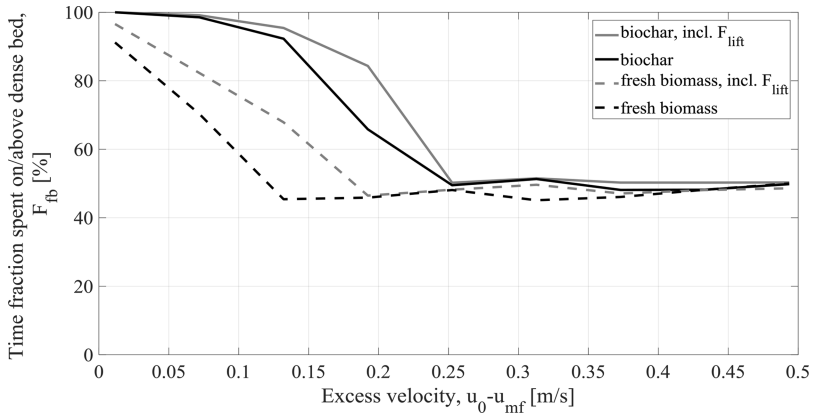

Figure 10. Modeled effect of the lift force on the time fraction that the fuel particles spent on and above the dense bed versus fluidization velocity. Fresh biomass and biochar, 4 cm in diameter, and μ_e = 1.23 Pa s.

fluidization velocity, seldom observation of the fuel particle outside the dense bed.

The influence of the model for bubble growth on the time fraction spent by the fuel particle on and above the dense bed surface was investigated. Three different bubble models[32,45,46] were tested, although the choice of model had very little effect on the axial mixing behaviors of the fuel particles.

The influence of the fuel-to-bubble velocity ratio, α, was also investigated. The values obtained in experiments, which vary over fluidization velocity (Figure 4), and the much lower values found in the literature, which remain constant over the fluidization velocity, were investigated. The influence of α on the axial mixing was significant only for low α values (approximately <0.15). This, together with the results of the sensitivity analysis shown in Figure 9, indicates that the dominating mechanisms in the emulsion zone have a major impact on the axial mixing of the fuel particle, while the model is less sensitive on the parameters in the bubble wake zone.

The effect on the immersion velocity (Figure 3) when including the lift force in the force balance suggests that the lift force has an influence on the axial mixing of the fresh biomass particles in the model. Figure 10 shows this effect of the lift force on the time fraction that the fuel particle spent on and above the dense bed versus fluidization velocity. When including the lift force, which is in the order of magnitude of the gravitational and buoyancy forces, the fuel particles spend significantly more time on the bed surface for fluidization velocities in the transition regime, as compared to a situation in which the lift force is excluded. As the drag of the bed solids on the fuel particle increases with increasing excess velocity, the effect of the lift force is reduced.

4.3. Modeling a Converting Biomass Particle. Finally, the model is used to simulate the axial mixing of a biomass particle that is undergoing drying, devolatilization, and char conversion. The fuel is assumed to be a spherical biomass particle with 8 wt % moisture and a carbon content of 47 wt % (typical value for biomass pellets produced from forest wood). Table 3 gives an overview of the input values for the model.

Figure 11 shows the probability that the converting biomass particle will be present in one of three areas (dense bed, bed surface, and splash zone) as conversion proceeds. The bed surface is defined as an area that includes the bed height of ±1 cm. The start of char conversion is indicated with dashed lines. The total modeling time is divided into timesteps of 30 s.

Table 3. Input Parameters for Modeling a Converting Biomass Particle

parameter	value
tracer initial diameter (D_i)	0.02 m
density of fresh biomass (ρ_I)	813 kg/m^3
density of char biomass (ρ_{II})	380 kg/m^3
time for volatilization (τ_{vol})	119 s
time for char conversion (τ_{ch})	214 s
timestep	10^{-4} s

https://dx.doi.org/10.1021/acs.energyfuels.9b04194
Energy Fuels 2020, 34, 3294−3304

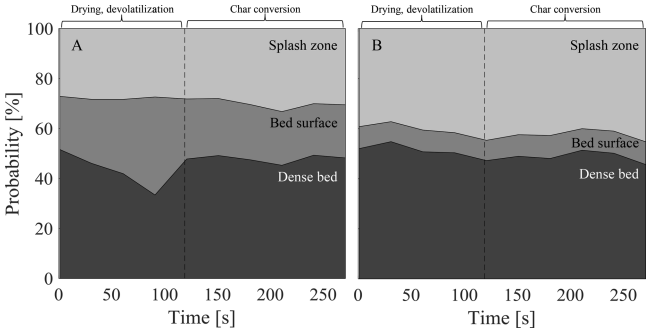

Figure 11. Probabilities of the biomass particle being present in the different areas of the bed over time. (A) Excess velocity, $u_0 - u_{mf}$ = 0.13 m/s. (B) Excess velocity, $u_0 - u_{mf}$ = 0.37 m/s.

With a smaller timestep of 10^{-4} s, the model is able to resolve the velocity of the particle until 99.8% of its original mass of char is converted. For a particle diameter of <3 mm, the timestep should be even smaller to resolve properly the mixing of the particle as it approaches full conversion. However, it should be noted that the char particle is probably elutriated into the freeboard once the diameter is sufficiently small. Figure 11A shows the probability distribution for an excess velocity of $u_0 - u_{mf}$ = 0.13 m/s. At this low fluidization velocity, the biomass particle exhibits a more flotsam behavior during drying and devolatilization (when the particle density is reduced), while the probability that the particle will be present in the splash zone does not change significantly. Once it enters the char conversion stage, the change in particle diameter has a little effect on the distribution between the three zones.

As depicted in Figure 11B, which shows the distribution for a higher excess velocity of $u_0 - u_{mf}$ = 0.37 m/s, the particle is less prone to float on the bed surface (cf. the lower fluidization velocity in Figure 11A). Instead, mixing into the dense bed is increased during drying and devolatilization, together with the time spent in the splash zone. This is a consequence of larger bubbles being formed, which enhance the movement of the bed material and cause more vigorous bubble eruptions. With the decreases in density and particle size as conversion advances, the time spent in the splash zone is slightly increased, which can be explained by the lighter particle being ejected higher up into the splash zone.

Figure 12 shows how an increase in excess velocity influences the probability of the biomass particle being located within the dense bed, bed surface, or splash zone, as obtained from the modeling. With increasing fluidization, the bubbles become bigger and the probability that the biomass particle will be mixed into the dense bed increases to around 50%, where it remains despite increasing fluidization velocity, while the time that the particle floats on the bed surface decreases significantly and the occurrence in the splash zone increases roughly linearly. The latter phenomenon can be explained as the growth of the bubbles causing a higher ejection velocity of the particle into the splash zone such that the particles reach higher up in the freeboard where they consequently spend longer time. The results shown in Figure 12 are qualitatively similar to those reported by Yang et al.,[47] who measured the mixing of biomass particles under conversion in a 2D bed under hot conditions.

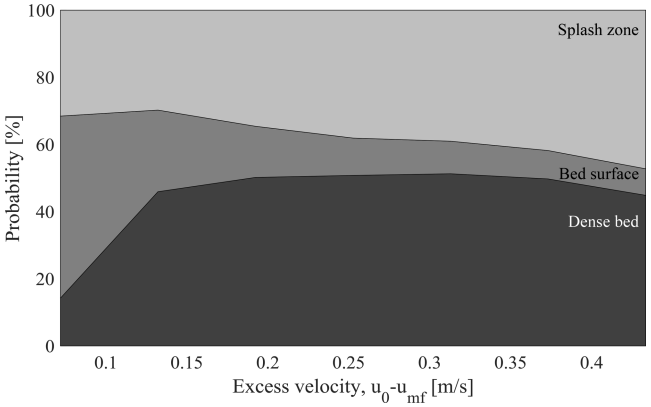

Figure 12. Probability of the total time for the biomass particle to be present in the different areas of the bed versus the excess velocity.

5. CONCLUSIONS

We show that the axial mixing of a fuel particle in the bottom region of a fluidized bed can be mathematically described in semiempirical modeling, giving good agreement with actual measurements. The model is based on the definition of two solid zones in the dense bed (bubble wake and emulsion) and one in the splash zone, each of which displays a characteristic flow pattern for the fuel particle. Of these zones, the mixing in the emulsion zone has the strongest impact on the final axial distribution of the fuel. In the emulsion zone, fuel mixing can be described in a satisfactory way by a force balance that considers both the buoyancy toward the bed emulsion and the drag force from the sinking bed material. Three parameters are found to be highly relevant for the axial fuel mixing: (i) the apparent viscosity of the emulsion, (ii) the bubble wake volume, and (iii) the rising velocity of the tracer in the bubble wake. The model shows good agreement with measurement values obtained for the three respective parameters: an apparent viscosity of 1.24 Pa s (taken from the literature[38]), a bubble wake volume ratio of 0.94 (fitted value), and a fuel-to-bubble velocity ratio that decreases from 0.94 to 0.55 with the fluidization velocity (taken from experiments conducted under fluid-dynamically scaled conditions[1]). Modeling the axial mixing of a biomass particle that is undergoing conversion yields results that are in agreement qualitatively with the experimental data from the literature regarding measurement in a pseudo-two-dimensional unit;[47] with decreasing density, the particle spends more time on the bed surface, while increasing the fluidization enhances axial mixing regardless of particle density or size.

AUTHOR INFORMATION

Corresponding Author

Anna Köhler − *Department of Space, Earth, and Environment, Chalmers University of Technology 412 96 Göteborg, Sweden;* orcid.org/0000-0002-4484-944X; Email: annaev@chalmers.se

Authors

David Pallarès − *Department of Space, Earth, and Environment, Chalmers University of Technology 412 96 Göteborg, Sweden*

Filip Johnsson − *Department of Space, Earth, and Environment, Chalmers University of Technology 412 96 Göteborg, Sweden*

Complete contact information is available at: https://pubs.acs.org/10.1021/acs.energyfuels.9b04194

https://dx.doi.org/10.1021/acs.energyfuels.9b04194
Energy Fuels 2020, 34, 3294−3304

Notes

The authors declare no competing financial interest.

■ ACKNOWLEDGMENTS

This work was financed by the Swedish Gasification Centre (SFC) within the framework of the Centre for Indirect Gasification of Biomass (CIGB) and by the Swedish Energy Agency within the framework of project P-38347-2.

■ NOTATION

Roman Letters

A_0 = bubble catchment area (m^2)
C_d = drag coefficient
D = diameter (m)
f_2 = empirical expression
F_{lift} = lift force (N)
f_w = bubble wake fraction
g = gravitational constant (m/s^2)
H_0 = fixed bed height (m)
m = mass of fuel particle (kg)
Q = released gas flow rate (m^3/s)
q = probability to start rising (%)
t = time (s)
u = velocity (m/s)
z = axial position (m)

Greek Letters

α = fuel-to-bubble velocity ratio
δ = bubble fraction
θ = ejection angle (°)
μ = apparent viscosity (Pa s)
ρ = density (kg/m^3)
τ = time (s)

Indices

b = bubble
br = single bubble
ch = char conversion
e = emulsion
im = immersion
mf = minimum fluidization
o = initial
p = fuel particle
s = bed solids
tr = throughflow
vol = devolatilization

■ REFERENCES

(1) Köhler, A.; Rasch, A.; Pallarès, D.; Johnsson, F. Experimental Characterization of Axial Fuel Mixing in Fluidized Beds by Magnetic Particle Tracking. *Powder Technol.* **2017**, *316*, 492−499.
(2) Koornneef, J.; Junginger, M.; Faaij, A. Development of Fluidized Bed Combustion—An Overview of Trends, Performance and Cost. *Prog. Energy Combust. Sci.* **2007**, *33*, 19−55.
(3) Geldart, D. Types of Gas Fluidization. *Powder Technol.* **1973**, *7*, 285−292.
(4) Svensson, A.; Johnsson, F.; Leckner, B. Bottom Bed Regimes in a Circulating Fluidized Bed Boiler. *Int. J. Multiph. Flow* **1996**, *22*, 1187−1204.
(5) Qin, K.; Thunman, H.; Leckner, B. Mass Transfer under Segregation Conditions in Fluidized Beds. *Fuel* **2017**, *195*, 105−112.
(6) Lundberg, L.; Tchoffor, P. A.; Pallarès, D.; Johansson, R.; Thunman, H.; Davidsson, K. Influence of Surrounding Conditions and Fuel Size on the Gasification Rate of Biomass Char in a Fluidized Bed. *Fuel Process. Technol.* **2016**, *144*, 323−333.
(7) Olsson, J.; Pallarès, D.; Johnsson, F. Lateral Fuel Dispersion in a Large-Scale Bubbling Fluidized Bed. *Chem. Eng. Sci.* **2012**, *74*, 148−159.
(8) Nienow, A. W.; Rowe, P. N.; Chiwa, T. Mixing and Segregation of a Small Proportion of Large Particles in Gas Fluidized Beds of Considerably Smaller Ones. *AIChE Symp. Ser.* **1978**, *74*, 45−53.
(9) Rios, G. M.; Dang Tran, K.; Masson, H. FREE OBJECT MOTION IN A GAS FLUIDIZED BED. *Chem. Eng. Commun* **1986**, *47*, 247−272.
(10) Lim, K. S.; Agarwal, P. K. Circulatory Motion of a Large and Lighter Sphere in a Bubbling Fluidized Bed of Smaller and Heavier Particles. *Chem. Eng. Sci.* **1994**, *49*, 421−424.
(11) Soria-Verdugo, A.; Garcia-Gutierrez, L. M.; Sanchez-Delgado, S.; Ruiz-Rivas, U. Circulation of an Object Immersed in a Bubbling Fluidized Bed. *Chem. Eng. Sci.* **2011**, *66*, 78−87.
(12) Soria-Verdugo, A.; Garcia-Gutierrez, L. M.; García-Hernando, N.; Ruiz-Rivas, U. Buoyancy Effects on Objects Moving in a Bubbling Fluidized Bed. *Chem. Eng. Sci.* **2011**, *66*, 2833−2841.
(13) Weinell, C. E.; Dam-Johansen, K.; Johnsson, J. E. Single-Particle Behaviour in Circulating Fluidized Beds. *Powder Technol.* **1997**, *92*, 241−252.
(14) Fotovat, F.; Ansart, R.; Hemati, M.; Simonin, O.; Chaouki, J. Sand-Assisted Fluidization of Large Cylindrical and Spherical Biomass Particles: Experiments and Simulation. *Chem. Eng. Sci.* **2015**, *126*, 543−559.
(15) Windows-Yule, C. R. K.; Moore, A.; Wellard, C.; Werner, D.; Parker, D. J.; Seville, J. P. K. Particle Distributions in Binary Gas-Fluidised Beds: Shape Matters−But Not Much. *Chem. Eng. Sci.* **2020**, *216*, 115440.
(16) Penn, A.; Boyce, C. M.; Conzelmann, N.; Bezinge, G.; Pruessmann, K. P.; Müller, C. R. Real-Time Magnetic Resonance Imaging of Fluidized Beds with Internals. *Chem. Eng. Sci.* **2019**, *198*, 117−123.
(17) Nikku, M.; Myöhänen, K.; Ritvanen, J.; Hyppänen, T.; Lyytikäinen, M. Three-Dimensional Modeling of Biomass Fuel Flow in a Circulating Fluidized Bed Furnace with an Experimentally Derived Momentum Exchange Model. *Chem. Eng. Res. Des.* **2016**, *115*, 77−90.
(18) Pallarès, D.; Johnsson, F. Macroscopic Modelling of Fluid Dynamics in Large-Scale Circulating Fluidized Beds. *Prog. Energy Combust. Sci.* **2006**, *32*, 539−569.
(19) Ratschow, L.; Wischnewski, R.; Hartge, E. U.; Werther, J. Three-Dimensional Simulation of Temperature Distributions in Large-Scale Circulating Fluidized Bed Combustors. In *Proceedings of the 20th International Conference on Fluidized Bed Combustion*; Yue, G., Zhang, H., Zhao, C., Luo, Z., Eds.; Springer Berlin Heidelberg: Berlin, Heidelberg, 2010; pp 780−785.
(20) Myöhänen, K.; Hyppänen, T. A Three-Dimensional Model Frame for Modelling Combustion and Gasification in Circulating Fluidized Bed Furnaces. *Int. J. Chem. React. Eng.* **2011**, DOI: 10.1515/1542-6580.2571.
(21) Köhler, A.; Pallarès, D.; Johnsson, F. Determination of the Apparent Viscosity of Dense Gas-Solids Emulsion by Magnetic Particle Tracking. In *23rd International Conference on Fluidized Bed Conversion*; Dept. of Space, Earth and Environment, Chalmers University of Technology: Seoul, South Korea, 2018.
(22) Sette, E.; Pallarès, D.; Johnsson, F. Experimental Quantification of Lateral Mixing of Fuels in Fluid-Dynamically down-Scaled Bubbling Fluidized Beds. *Appl. Energy* **2014**, *136*, 671−681.
(23) Kunii, D.; Levenspiel, O. *Fluidization Engineering*; Butterworth-Heinemann, 1991.
(24) Rowe, P. N.; Partridge, B. A. An X-Ray Study of Bubbles in Fluidised Beds. *Chem. Eng. Res. Des.* **1997**, *75*, S116−S134.
(25) Davidson, J. F.; Harrison, D. *Fluidised Particles*. Cambridge University Press: New York 1963.
(26) Grace, J. R.; Harrison, D. The Behaviour of Freely Bubbling Fluidised Beds. *Chem. Eng. Sci.* **1969**, *24*, 497−508.
(27) Grace, J. R.; Clift, R. On the Two-Phase Theory of Fluidization. *Chem. Eng. Sci.* **1974**, *29*, 327−334.

https://dx.doi.org/10.1021/acs.energyfuels.9b04194
Energy Fuels 2020, 34, 3294−3304

(28) Werther, J. Influence of the Bed Diameter on the Hydrodynamics of Gas Fluidized Beds. In *AIChE symposium series*; 1974; Vol. *70*, pp 53−62.
(29) Johnsson, F.; Andersson, S.; Leckner, B. Expansion of a Freely Bubbling Fluidized Bed. *Powder Technol.* **1991**, *68*, 117−123.
(30) Davies, R. M.; Taylor, G. The Mechanics of Large Bubbles Rising through Extended Liquids and through Liquids in Tubes. *Proc. R. Soc. London, Ser. A* **1997**, *200*, 375−390.
(31) Rowe, P. N.; Nienow, A. W. Particle Mixing and Segregation in Gas Fluidised Beds A Review. *Powder Technol.* **1976**, *15*, 141−147.
(32) Darton, R. C.; La Nauze, R.; Davidson, J. F.; Harrison, D. Bubble Growth Due To Coalescence in Fluidized Beds. *Trans. Inst. Chem. Eng.* **1977**, *55*, 274−280.
(33) Baeyens, J.; Wu, S. Y. Bed Expansion and the Visible Bubble Flow Rate in Gas Fluidized Beds. *Adv. Powder Technol.* **1992**, *3*, 163−189.
(34) Crowe, C. T.; Schwarzkopf, J. D.; Sommerfeld, M.; Tsuji, Y. *Multiphase Flows with Droplets and Particles*, Second Edi. ; 2011, DOI: 10.1201/b11103.
(35) Garcia-Gutierrez, L. M.; Soria-Verdugo, A.; Marugán-Cruz, C.; Ruiz-Rivas, U. Simulation and Experimental Study on the Motion of Non-Reacting Objects in the Freeboard of a Fluidized Bed. *Powder Technol.* **2014**, *263*, 112−120.
(36) Rowe, P. N.; Partridge, B. A.; Cheney, A. G.; Henwood, G. A.; Lyall, E. The Mechanisms of Solids Mixing in Fluidised Beds. *Chem. Eng. Res. Des.* **1965**, *43a*, 271−286.
(37) Schiller, L.; Naumann, A. Über Die Grundlegenden Berechnungen Bei Der Schwerkraftaufbereitung. *Verein Dtsch. Ingenieure* **1933**, *44*, 318−320.
(38) Rees, A. C.; Davidson, J. F.; Dennis, J. S.; Hayhurst, A. N. The Apparent Viscosity of the Particulate Phase of Bubbling Gas-Fluidized Beds: A Comparison of the Falling or Rising Sphere Technique with Other Methods. *Chem. Eng. Res. Des.* **2007**, *85*, 1341−1347.
(39) Solimene, R.; Marzocchella, A.; Salatino, P. Hydrodynamic Interaction between a Coarse Gas-Emitting Particle and a Gas Fluidized Bed of Finer Solids. *Powder Technol.* **2003**, *133*, 79−90.
(40) Kumar, R. R.; Kolar, A. K.; Leckner, B. Effect of Fuel Particle Shape and Size on Devolatilization Time of Casuarina Wood. In *Science in Thermal and Chemical Biomass Conversion*; CPL Press: Victoria, Vancouver Island, BC, Canada, 2004; pp 1251−1264.
(41) Köhler, A.; Pallarès, D.; Johnsson, F. Magnetic Tracking of a Fuel Particle in a Fluid-Dynamically down-Scaled Fluidised Bed. *Fuel Process. Technol.* **2017**, *162*, 147.
(42) Sette, E.; Pallarès, D.; Johnsson, F.; Ahrentorp, F.; Ericsson, A.; Johansson, C. Magnetic Tracer-Particle Tracking in a Fluid Dynamically down-Scaled Bubbling Fluidized Bed. *Fuel Process. Technol.* **2015**, *138*, 368−377.
(43) Glicksman, L. R.; Hyre, M. R.; Farrell, P. A. Dynamic Similarity in Fluidization. *Int. J. Multiphase Flow* **1994**, *20*, 331−386.
(44) Rees, A. C.; Davidson, J. F.; Dennis, J. S.; Hayhurst, A. N. The Rise of a Buoyant Sphere in a Gas-Fluidized Bed. *Chem. Eng. Sci.* **2005**, *60*, 1143−1153.
(45) Bauer, W.; Werther, J.; Emig, G. Der Einfluß Der Gasverteiler-Konstruktion Auf Das Betriebsverhalten von Wirbelschichten. *Chem. Ing. Tech.* **1981**, 202−203.
(46) Mori, S.; Wen, C. Y. Estimation of Bubble Diameter in Gaseous Fluidized Beds. *AIChE J.* **1975**, *21*, 109−115.
(47) Yang, Z.; Duan, L.; Li, L.; Liu, D.; Zhao, C.. Movement and Mixing Behavior of a Single Biomass Particle during Combustion in a Hot Fluidized Bed Combustor. *In the Fluidization XVI Conference*; Guilin, China, 2019.

https://dx.doi.org/10.1021/acs.energyfuels.9b04194
Energy Fuels 2020, 34, 3294−3304